Non-parametric reconstruction of the galaxy-lens in PG1115+080

Prasenjit Saha
Department of Physics (Astrophysics)
Keble Road, Oxford OX1 3RH
saha@physics.ox.ac.uk

Liliya L.R. Williams
Institute of Astronomy
Madingley Road, Cambridge CB3 0HA
llrw@ast.cam.ac.uk

Abstract: We describe a new, non-parametric, method for reconstructing lensing mass distributions in multiple-image systems, and apply it to PG1115+080, for which time delays have recently been measured.

It turns out that the image positions and the ratio of time delays between different pairs of images constrain the mass distribution in a linear fashion. Since observational errors on image positions and time delay ratios are constantly improving, we use these data as a rigid constraint in our modelling. In addition, we require the projected mass distributions to be inversion-symmetric and to have inward-pointing density gradients. With these realistic yet non-restrictive conditions it is very easy to produce mass distributions that fit the data precisely.

We then present models, for $H_0 = 42$, 63 and 84 $\mathrm{km\,s^{-1}\,Mpc^{-1}}$, that in each case minimize mass-to-light variations while strictly obeying the lensing constraints. (Only a very rough light distribution is available at present.) All three values of H_0 are consistent with the lensing data, but require quite different morphologies for the lensing galaxy. If H_0 is low, the main lensing galaxy could be an early type. If H_0 is high, the galaxy is reconstructed as a late elliptical or nearly edge-on disc; a binary or merging system is also plausible.

1. INTRODUCTION

Observational data permitting, it is always better to model physical systems non-parametrically, so as not to impose our prejudices and preconceptions on the outside world. In cases of limited observational constraints, a non-parametric model is not an option: one needs a parametric model to fill in the gaps left by our observational ignorance.

To date, all models of multiply-imaged QSOs are parametric, i.e., based on a predefined model for the galaxy mass distribution, like an isothermal sphere, de Vaucouleurs profile, King profile, etc., (For example, see Kochanek 1991.) The parameters of the model are determined by optimizing the fit between the observables and the corresponding model-predicted values, like image positions. The reason for using parametric models is that the number of observables is usually small and there is no need to go beyond parametric models. However, lately it has become apparent (Witt & Mao 1997) that parametric elliptical lenses are not adequate for modeling quadruple-lens systems, i.e., no lens with well determined image positions is satisfactorily fit by an isolated elliptical galaxy lens.

The history of modeling of PG1115+080 is an illustrative example of how lens modeling has evolved in the last 15 years or so. The first published model of PG1115 (Young *et al.* 1981) considered a spiral galaxy-lens consisting of a highly flattened disk and a slightly flattened bulge. Since the two components had different velocity dispersions, scale lengths, and ellipticities, the model had six parameters even without the adjustable lens redshift. There were only six observational constraints. The acceptability of this over-specified yet realistic model went to show that the image configuration could easily arise from gravitational lensing. Later modelers demonstrated that the image configuration could be achieved with less parameters; Narasimha *et al.* (1983) used a single component lens: a truncated, mildly elliptical King profile. Kochanek (1991) fit five different models, each with 5 free parameters. With the arrival of more observational constraints, i.e. the galaxy position, more precise image positions (Kristian *et al.* 1993, hereafter K93, Courbin *et al.* 1997), and time delays for the images (Schechter *et al.* 1997, hereafter S97), all the single galaxy parametric models became unacceptable (S97, Keeton & Kochanek 1997).

A very plausible explanation is that nearby external galaxies contribute non-negligible shear, and possibly convergence at the location of the images. Adding external galaxies gives one at least two additional parameters, magnitude and position angle of the shear, and thus more freedom to fit the data. This approach has been explored by Witt & Mao (1997), and Keeton & Kochanek (1997).

A reasonable question to ask is, as the observational constraints tighten should one use more elaborate parametric models with more free parameters to get acceptable fits to the observations? How far can one justify this approach?

Instead, we decided to explore non-parametric models of the galaxy mass distribution. In this paper we describe our modeling method and apply it to a quadruple gravitational lens system, PG1115+080. We show that the lensing observational constraints in this system (image positions and time delay ratio), combined with a few general, non-restrictive requirements for the galaxy mass distribution produce realistic galaxy models.

Our original motive for pursuing the non-parametric approach was to place realistic limits on the value of H_0, as derived from the time delays in the quadruple

PG1115 system. It has been pointed out by many authors that H_0 determination from a multiple-image lens system is preferable to the conventional distance ladder approach (Jacoby *et al.* 1992) since the former measures H_0 on truly cosmological scales, thereby avoiding any mass inhomogeneities in the local Universe, and bypassing all the rungs in the distance ladder with their respective uncertainties. The lensing method is not without its own problems; the derived value of H_0 is sensitive to the uncertain mass distribution in the lens. Thus far only parametric mass models of PG1115 have been considered in the literature. However, there is always a worry with parametric models that only a small piece of the whole allowable model space is being looked at, so errors in the derived mass model, and consequently errors in H_0 would be underestimated. In fact, our modeling clearly shows that the current parametric models do not cover all the possible realistic galaxy mass distributions, since our derived galaxy masses look different from the existing parametric models. An example of models that are realistic but are not allowed by the existing single-galaxy parametric models are mass distributions with twisting iso-density contours.

2. OBSERVATIONS OF PG1115+080

PG1115+080 was the second multiply-imaged QSO to be discovered (Weymann *et al.* 1980). It was originally selected as a QSO candidate based on its UV excess, and later spectroscopically confirmed and entered into the bright Palomar-Green QSO sample (Green, Schmidt, Liebert 1986). Its redshift, based on several emission lines, is $z = 1.722$; its magnitude is $V = 15.8$. The multiple nature of PG1115 first became apparent during the observations of Weymann *et al.*, when during brief periods of good seeing images B and C were resolved by the TV guiding monitor at the 2.3-m at Steward Observatory. Soon after, image A was shown to consist of two images 0.5 arcseconds apart (Hege *et al.* 1981).

Several imaging observations were carried out on PG1115, but to date, the best astrometry on the system is from WFPC HST observations reported by K93, and from NOT and CFHT observations reported by Courbin *et al.* (1997). We will use the positions from K93 in this paper, but results using the Courbin *et al.* astrometry are nearly identical.

Even though it was recognized early on that the geometry of image configuration can be reproduced by a single lensing galaxy (Young *et al.* 1981), the identity and location of the galaxy remained elusive for several years. The galaxy was eventually identified by Shaklan & Hege (1986), Christian *et al.* (1987), and K93. It turned out to be a rather red faint object, $R \sim 20$, and $V - R \sim 0.7$, situated between the QSO images, and somewhat closer to B. In addition to the main lensing galaxy, a nearby group of 3 galaxies was found about 10–20 arcseconds south-west of PG1115 (Young *et al.* 1981, Henry & Heasley 1986). Henry & Heasley (1986) obtained the redshifts of the two brighter galaxies, $z = 0.305$; while Angonin-Willaime *et al.* (1993) determined the redshift of the main lensing galaxy to be 0.295 ± 0.005. Just recently, Kundić *et al.* (1997) and Tonry (1997) obtained Keck spectra for all four group galaxies, and showed that they are all at $z = 0.311$, and belong to a group with a line-of-sight velocity dispersion of 270 ± 40 km s^{-1}, and properties similar to those of Hickson's compact groups. Here, we will assume that the lensing galaxy is at $z = 0.311$, and its position is as given in K93. As yet the lensing galaxy's morphological type is unknown,

but it is probably an elliptical because (1) the image positions very robustly require $\sim 10^{11} h^{-1} M_\odot$ within a radius of $3h^{-1}$ kpc; (2) the galaxy spectrum (Kundić *et al.* 1997) shows no emission lines that would be indicative of a merger or ongoing star-formation; (3) Tonry (1997) measures the velocity dispersion of the galaxy to be 281–293 km s^{-1}, depending on the aperture correction.

Unlike the 2-image QSO 0957+561, there is probably no other significant mass concentrations along the line of sight to PG1115. Based on IUE data, Tripp *et al.* (1990) report that there is no high column density Lyman-α absorption in the QSO spectrum, above the redshift of 0.39. Thus we assume that all the mass relevant to lensing calculations is in a single screen at $z = 0.311$.

There have been a number of reports of image variability in this system (Vanderriest *et al.* 1986, Foy *et al.* 1985, Michalitsianos *et al.* 1996). These observations were done under varying conditions, by a number of observers using different filters and instruments, and with large time lags between data points. As was pointed out by K93, the heterogeneous nature of accumulated data precludes one from making any positive conclusion regarding image variability either between images, or between same images at different epochs.

Recently, S97 obtained a set of homogeneous photometric data on the A1+A2, B, and C images of PG1115 on 30 nights that span a period of about 200 days in 1995-1996. The noise level varies from 4 millimag for combined images A1+A2, to 13 millimag for image B. The lightcurves show systematic variations of sufficiently large amplitude, $\Delta m \sim 0.15$ mag, to derive relative time delays between images. A preliminary evaluation of time delays by S97 was soon followed by another analysis of the same data by Bar-Kana (1997; hereafter BK97), who incorporated the possible effects of correlated errors and microlensing. BK97 estimates that B lags C by $25^{+3.3}_{-3.8}$ days, consistent with the S97's 23.7 ± 3.4 days. The delay between B and A is less certain, ~ 10–14 days. The ratio between time delays consequently remains somewhat uncertain; BK97 estimates $t_{\rm AC}/t_{\rm BA} = 1.13^{+0.18}_{-0.17}$ compared with S97's $\simeq 0.6$. We will use the S97 values for one reconstruction in this paper, but mostly we will work with the BK97 values.

Since the images are superimposed on the central part of the lensing galaxy, the optical image fluxes probably suffer from microlensing. This precludes one from using the optical flux ratios as a modeling constraint. Radio emission from a QSO would not be affected by microlensing, but PG1115 is radio-quiet, i.e. it is not detected down to 15 mJy level with the VLA (Weymann *et al.* 1980). However, even if microlensing-free radio flux ratios existed, they would not provide a good model constraint: between the time delays, image positions and image amplifications, the latter are the most sensitive to small changes in the lensing model. This is because image fluxes are a function of the second derivative of the 2D lensing potential, whereas the time delays and image positions are proportional to the lensing potential and its first derivative, respectively. (See also Section 3.) We do not use image fluxes ratios as constraints in our modeling.

To sum up, PG1115+080 is a quadruply-lensed bright optical QSO, with well defined image positions (5 mas errorbars or better), a dominant lensing galaxy (50 mas position errorbars or better), and well constrained and easily observable time delays of $\sim$ several days to a couple of weeks.

Before we proceed we would like to emphasize that not all observational constraints are equally good for the purposes of lens modeling, even if the observational errors are

small. The best observables are the ones that depend on the global properties of the lens, with little sensitivity to local mass variations. As we already mentioned, image fluxes are not reliable for that reason, while image positions are more stable. Time delays between images are also very good, but since time delays themselves involve H_0, we use the *ratio* of the two observed time delays, t_{AC}/t_{BA}. Thus we have 9 constraints: 8 from image positions, plus the time delay ratio. In principle, the errors on these quantities will keep on shrinking with improving data. Therefore, we use these data as rigid constraints.

3. A LENS RECONSTRUCTION METHOD

Here we describe our method of non-parametrically reconstructing the galaxy mass distribution based on observed lensing constraints, and a few general requirements for the galaxy. We take the lens as a pixellated mass distribution. It is simplest to leave masses in terms of the critical density, so we say that the nth pixel has surface density κ_n times

$$\Sigma_{\text{crit}} = \frac{D_\text{L} D_\text{S}}{D_\text{LS}} \frac{c^2}{4\pi G},$$ (1)

Σ_{crit} being the critical surface mass density for lensing in units of mass per unit solid angle at the redshift of the lens. The nth pixel's contribution to the potential at some $\boldsymbol{\theta}$ is $\kappa_n \psi_n(\boldsymbol{\theta})$ and its contribution to the bending angle is $\kappa_n \boldsymbol{\alpha}_n(\boldsymbol{\theta})$, where

$$\begin{aligned} \psi_n(\boldsymbol{\theta}) &= \frac{1}{\pi} \int \ln |\boldsymbol{\theta} - \boldsymbol{\theta}'| \, d^2\boldsymbol{\theta}', \\ \boldsymbol{\alpha}_n(\boldsymbol{\theta}) &= \frac{1}{\pi} \int \frac{\boldsymbol{\theta} - \boldsymbol{\theta}'}{|\boldsymbol{\theta} - \boldsymbol{\theta}'|^2} \, d^2\boldsymbol{\theta}'. \end{aligned}$$ (2)

The integrals in (2) are over the n-th pixel, and depend on where $\boldsymbol{\theta}$ is relative to that pixel, and on the pixel size (say a). Explicit expressions ψ_n and $\boldsymbol{\alpha}_n$ for square pixels are worked out in the Appendix.

To get the full time delay and bending angle we sum over all pixels. For a source at $\boldsymbol{\theta}_\text{S}$ the time delay is proportional to

$$\tau(\boldsymbol{\theta}) = \tfrac{1}{2}|\boldsymbol{\theta}|^2 - \boldsymbol{\theta} \cdot \boldsymbol{\theta}_\text{S} - \sum_n \kappa_n \psi_n(\boldsymbol{\theta}).$$ (3)

(Compared to how (3) is usually written, we have dropped the term $\tfrac{1}{2}|\boldsymbol{\theta}_\text{S}|^2$ because it cancels for all observable effects.) To get the time delay in physical units we have to multiply τ by

$$(1 + z_\text{L}) \frac{D_\text{L} D_\text{S}}{c D_\text{LS}}.$$ (4)

Images will appear where $\nabla \tau(\boldsymbol{\theta}) = 0$, or

$$\boldsymbol{\theta} - \boldsymbol{\theta}_\text{S} - \sum_n \kappa_n \boldsymbol{\alpha}_n(\boldsymbol{\theta}) = 0.$$ (5)

Now, consider what lensing data imply when inserted into equations (3) and (5). First, the image positions in a multiple-image system tell us that $\nabla\tau(\boldsymbol{\theta}_i) = 0$ for some known $\boldsymbol{\theta}_i$. Each image provides two such constraint equations. From (5) we can see that these constraint equations are linear in the unknowns (κ_n and $\boldsymbol{\theta}_{\mathrm{S}}$). Secondly, if time delays have been measured between more than one pair of images, as in S97, then the ratio of time delays provides a constraint of the type

$$\tau(\boldsymbol{\theta}_4) - \tau(\boldsymbol{\theta}_1) = \langle\mathrm{ratio}\rangle \times (\tau(\boldsymbol{\theta}_2) - \tau(\boldsymbol{\theta}_1)). \tag{6}$$

Comparing with (3), we see that such constraints are also linear.

Thus the lensing data on PG1115+080 provide nine constraint equations, eight from the image positions and one from the time delay ratio. We will supplement these with some more constraints on physical grounds.

(i) Obviously, the κ_n must be non-negative.

(ii) The centroid of the lensing galaxy is known from K93, and we require the mass profile to be 180° rotation symmetric about this centroid. In other words $\kappa_{i,j} = \kappa_{-i,-j}$, where we are changing notation briefly from κ_n to $\kappa_{i,j}$ and $\kappa_{0,0}$ is centred on the galaxy centroid. We remark that without this constraint or some other that fixes the origin, the lensing data would have supplied only seven constraint equations.

(iii) For a galaxy we expect the density gradient to generally be pointing inwards. Accordingly, we define a pixellated density gradient

$$\nabla\kappa_{i,j} \equiv (2a)^{-1}\left(\kappa_{i+1,j} - \kappa_{i-1,j}\,,\ \kappa_{i,j+1} - \kappa_{i,j-1}\right) \tag{7}$$

and require that $\nabla\kappa_{i,j}$ point no more than 45° away from radially inwards.

(iv) We require that $\tau(\mathrm{A}1) < \tau(\mathrm{A}2)$, i.e., of the two A images, the southern one leads.[1]

(v) Though one can generate a mass profile and then calculate the implied H_0, in practice we found it more convenient to set H_0 at various values and generate different mass profiles at each value. Since the time scale (4) is $\propto H_0^{-1}$, fixing H_0 is just another linear constraint.

The foregoing are all linear equality and inequality constraints and it is straightforward to find, by linear programming, if there are any feasible mass distributions. If there are then there is not one mass model but a huge family of them, all consistent with the lensing data and our additional imposed constraints. At this point there are several sensible things one can do. One might take some sort of average over all the allowed mass distributions. Or one might specify some figure of merit such as smoothness or entropy, and then optimize subject to all the above constraints. In this paper we will do the latter, choosing our optimal model as the one with minimum mass-to-light variation. More precisely, given a pixellated light distribution L_n for the galaxy, we find the mass distribution that minimizes

$$\sum_n (\kappa_n - KL_n)^2, \quad \text{where } K = \sum_n \kappa_n,\ \sum L_n = 1, \tag{8}$$

---

[1] Given that C leads A leads B, there are two natural five-image configurations. One of them has A1, A2 and C as respectively minimum, saddle-point and mininum in a lemniscate, and B and the demagnified central image being respectively saddle-point and maximum in a limaçon. The other configuration has A1, A2 and C as respectively saddle-point, maximum and mininum in a limaçon. (See Figure 6 in Blandford and Narayan 1986.) Both of these have A1 leading A2, and in fact we have only ever seen the former in models of the PG1115 system. Other configurations are logically possible, but would have contorted time delay surfaces.

subject to all the linear constraints above.

Our reconstruction procedure has a simple geometrical interpretation. Supposing there are N independent pixels, consider the N-dimensional space of the independent κ_n. The lensing constraints and H_0 specification confine allowed models to a $(N-8)$-dimensional hyperplane in this space. (There are ten equality constraints in all, but two of them go to solve for $\boldsymbol{\theta}_{\mathrm{S}}$.) The inequality constraints further confine allowed models to a convex region of the hyperplane. Now L_n is a point in the N-dimensional space, and a line from the origin through L_n represents constant mass-to-light models. Our optimal model is then the point on the allowed part of the $(N-8)$-hyperplane that is closest to that line.

The numerical problem has a unique solution, and quadratic programming algorithms reliably find it. We used the NAG routine E04NFF.

In this paper we do not use flux ratios as additional constraints, because they are sensitive to local variations of κ rather than global variations and are thus weakly coupled to time delays, as was explained in Section 2. Therefore we did not attempt to constrain local variations of κ in our mass reconstructions, and in fact our mass maps have unphysically large pixel-to-pixel variation. This pixel-to-pixel noise does not matter for image positions and time delays because the potential remains very smooth (see Section 4 below), but it makes the magnification unphysically noisy. In principle, flux ratio fitting could be introduced into the reconstruction method in a straightforward way. Since inverse magnification involves products of the derivatives of the lens equation (5) it will be quadratic in the unknowns, and hence constraints involving magnification could be dealt with by the same numerical algorithms. But to avoid a situation where flux ratios just get fitted with pixel-to-pixel noise, it would be necessary to suppress the latter using suitable physically motivated constraints.

Is pixellating the mass distribution the best approach to non-parametric reconstruction? We don't know. Other strategies using either basis functions or grids with interpolation are certainly possible; these would avoid discontinuities in the mass distribution, and small scale inhomogeneities will be easier to suppress, but non-negativity may be much harder to enforce. But pixels have a certain conceptual simplicity, and mainly for this reason we decided that pixels should at least be investigated first.

4. RECONSTRUCTIONS OF THE LENS

For the PG1115 system, the time scale factor (4) equals $31h^{-1}$ days arcsec^{-2} for $q_0 = \frac{1}{2}$. The q_0 dependence is weak and is easily read off Figure 1, so in the text we will write "$h = 0.5$" as shorthand for "$H_0 = 50$ km s^{-1} Mpc^{-1} for $q_0 = \frac{1}{2}$" and so on. The angular diameter distance of the lens is $D_{\mathrm{L}} = 2.77h^{-1}$ kpc arcsec^{-1} and the critical density $\Sigma_{\mathrm{crit}} = 3.30h^{-1} \times 10^{10} M_{\odot}$ arcsec^{-2}. The total mass in a pixellated reconstruction is

$$\Sigma_{\mathrm{crit}} \times a^2 \sum_n \kappa_n. \tag{9}$$

We can define a formal Einstein radius θ_{E} by equating $a^2 \sum_n \kappa_n$ to $\pi \theta_{\mathrm{E}}^2$. (It is only formal because the lensing mass isn't circular and doesn't produce Einstein rings.) Then the total mass is

$$\theta_{\mathrm{E}}^2 \times 1.04 \times 10^{11} h^{-1} M_{\odot} \text{ arcsec}^{-2}. \tag{10}$$
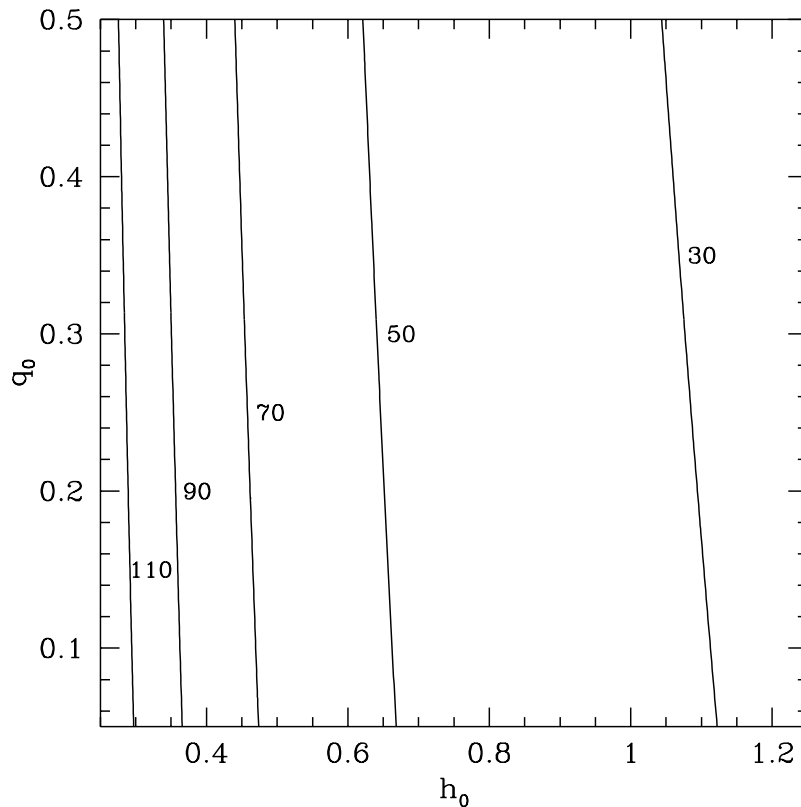
Figure 1. Contours of constant time delay in the q_0 vs. h_0 plane, expressed as the time factor given by equation (4). Contour lines are labelled in units of days arcsec^{-2}.

We can use equation (10) to associate formal Einstein rings with the other group galaxies too; it's a convenient way to show various masses on a figure.

In this section, we illustrate four reconstructions in detail. All have $0.1''$ mass pixels and confine the main lensing galaxy to a circle of radius $2''$ around the centroid measured by K93. (That makes 1265 pixels, but only 633 are independent because of the $180°$ rotation symmetry condition.) The other group galaxies, if they are included, are considered as three point masses. We did not find our reconstructions sensitive to the pixel size and maximum galaxy radius. For the light distribution against which we optimize we used the K93 model

$$L(\boldsymbol{\theta}) = \left(1 + \frac{|\boldsymbol{\theta}|^2}{\theta_0^2}\right)^{-\gamma/2}, \quad \theta_0 = 0.71'', \ \gamma = 1.7. \tag{11}$$

Again, our reconstructions are not very sensitive to the precise values of θ_0 and γ.

Figure 2 shows a minimum mass-to-light variation model that fits the astrometry from K93 and the time delays from S97 (C leads B by 23.7 days and A by 9.4 days) with $h = 0.5$. (This model does not include the other group galaxies, but their positions are indicated in the figure.) S97 fitted several parametric models to these data, finding that unless shear from the external galaxies was included the fits to the image positions were very poor, while the predicted time delay ratio was inconsistent ($\simeq 1.5$ versus $\simeq 0.6$) even with external shear. Keeton & Kochanek (1997) subsequently fitted more parametric models, with similar results. But for non-parametric models such difficulties evaporate; it is easy to fit all the lensing data precisely, even without external shear.
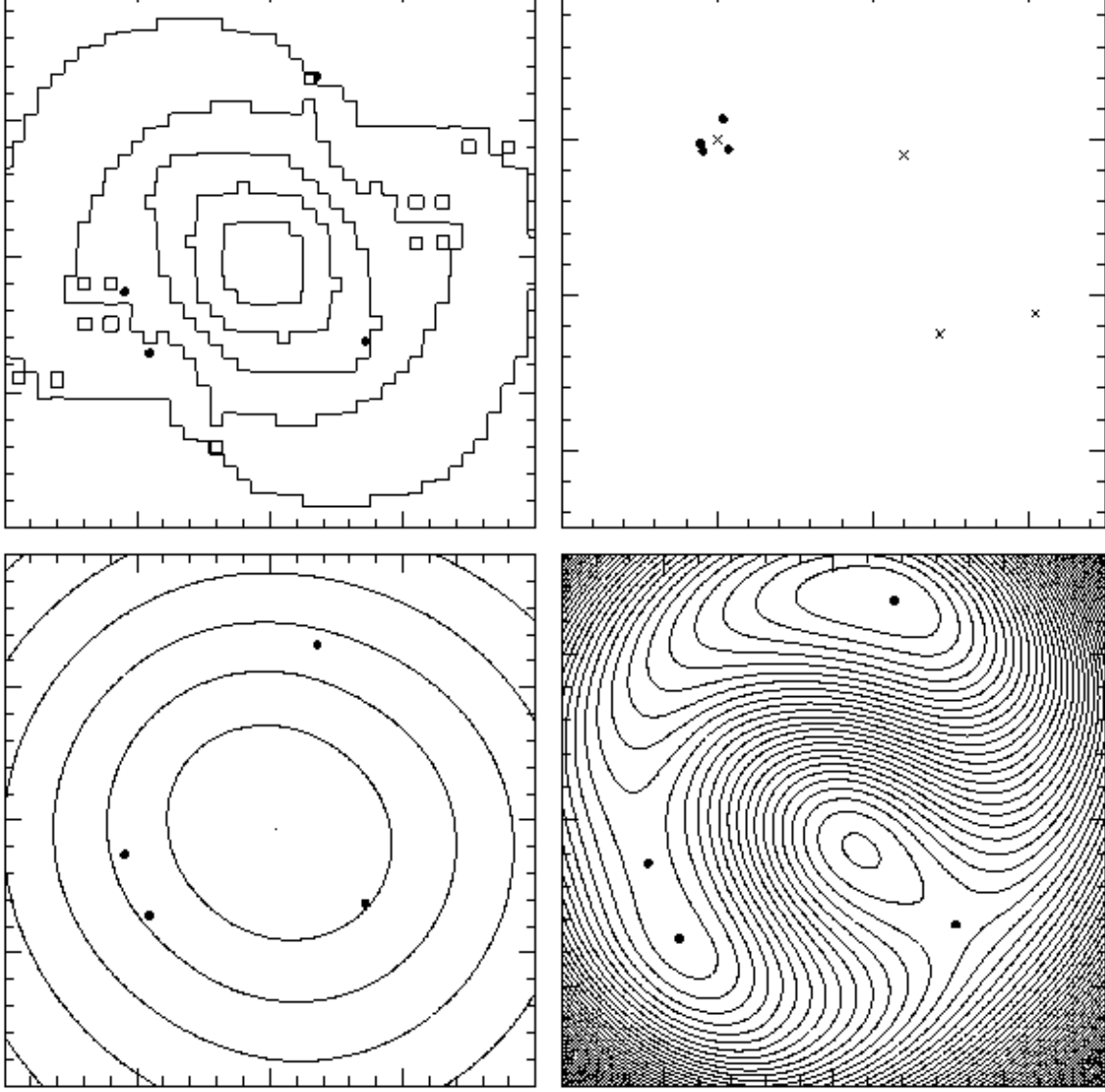
Figure 2.   A reconstruction constrained by the image positions from K93 and the time delays from the S97 analysis, and by $h = 0.5$.

We have suppressed axis labels to reduce clutter, but the image positions (marked by filled circles) in each panel should make the scales clear.

Upper left panel: Contours of the dimensionless surface density $\kappa = \frac{1}{3}, \frac{2}{3}, \ldots$, increasing inwards. The field shown is $(-2'', -2'')$ to $(2'', 2'')$ with the galaxy centroid from K93 at the origin.

Lower left panel: Contours of $\boldsymbol{\theta} \cdot \boldsymbol{\theta}_{\mathrm{S}} + \psi(\boldsymbol{\theta})$, increasing outwards in steps of $\frac{1}{2}$ arcsec^2. The field is as in the upper panel.

Lower right panel: Time delay contours, in steps of 1 day. The field shown is $(-1.6'', -1.6'')$ to $(1.6'', 1.6'')$ with the same origin.

Upper right panel: The field shown here is $(-10'', 25'')$ to $(-25'', 10'')$ relative to the same origin as before. The crosses mark the main lensing galaxy and the other group galaxies; the latter are not included in this reconstruction, but will be in later ones.

Though the model in Figure 2 is not one of the main results of this paper (because

the external galaxies have been omitted) it will do to illustrate the reconstruction method, so let us discuss the figure in some detail.

Density map: The 180° rotation symmetry allows isodensity contours to twist, and this seems to be a generic feature of our reconstructions though it is not always as pronounced as in this model. Some parametric models get a similar effect by using two shear axes. (Incidentally, the single-pixel peaks in the density map may seem inconsistent with our density gradient constraint. But because $\nabla \kappa_{ij}$ is formulated as a symmetric difference in equation 7, such single-pixel blemishes are in fact tolerated by the constraint.)

Lens potential: We plot $\boldsymbol{\theta}_{\mathrm{S}} \cdot \boldsymbol{\theta} + \psi(\boldsymbol{\theta})$ rather than $\psi(\boldsymbol{\theta})$ itself. Comparing with models that include the external galaxies, we have found that both $\boldsymbol{\theta}_{\mathrm{S}}$ and $\psi(\boldsymbol{\theta})$ change drastically on including those galaxies, but $\boldsymbol{\theta}_{\mathrm{S}} \cdot \boldsymbol{\theta} + \psi(\boldsymbol{\theta})$ (like the time delay surface) changes very little. In a sense there is a degeneracy between $\boldsymbol{\theta}_{\mathrm{S}}$ and the mass distribution, and in the plot we have used it to nominally move the source to the origin. It is remarkable how much smoother the potential is than the density; of course the smoothness comes from having integrated the density twice with a $\ln |\boldsymbol{\theta} - \boldsymbol{\theta}'|$ kernel.

Time delay contours: We have spaced the contours by 1 day, and this plot provides a pleasing visual check that our fitting program does what it is supposed to do. From this plot the central image may seem worryingly bright, but this is not really an issue. The reconstructions in this paper all have wide cores simply because the simple K93 light model does. But we could imagine reshaping the core in a circularly symmetric way to have a central density cusp; this would demagnify the central image without affecting the positions or time delays of the other images.

Now we discuss the reconstructions in Figures 3–5, which form the main results of this paper. These use the time delays $t_{\mathrm{BC}} = 25.0$ days and $t_{\mathrm{AC}}/t_{\mathrm{BA}} = 1.13$ from BK97's re-analysis of the S97 data, and include the other group galaxies as point masses. On the basis of the magnitudes in K93 we loosely constrained the allowed mass range of these galaxies (usually known as G1, G2, G3) relative to the main lensing galaxy G as follows: (i) The total mass of G1, G2 and G3 is no more than 10 times that of G; (ii) each of G1, G2 and G3 has more mass than G; (iii) G1 has more mass than G2 and G3 put together; (iv) G2 and G3 are at most a factor of 2 apart in mass. The masses of the galaxies, one of the outputs of the code, are proportional to the area of the circle in the diagrams.

As we already pointed out, realistic galaxy profiles are easy to obtain with our method, hence h is not usefully constrained by the current observations in this lens system. Since this is the case, we decided to carry out mass reconstructions for three plausible values of h. Figure 3 is constrained by $h = 0.42$, Figure 4 by $h = 0.63$ and Figure 5 by $h = 0.84$. We chose these values to coincide with the range found by S97 in their modelling.

The mass distribution looks different in the three cases. For $h = 0.42$, the galaxy is reconstructed as a possible early-type, or a face-on spiral. For $h = 0.84$, the galaxy is rather elongated, and so could be an edge-on disc, or highly flattened elliptical. Note that in all three cases, the major axis is aligned with the major axis of the group. The effect is barely noticeable for a low Hubble constant (see outer isophotes in Figure 3), and is most pronounced for a high Hubble constant. Is this alignment physically motivated? It is generally observed that brightest cluster galaxies (BCGs)
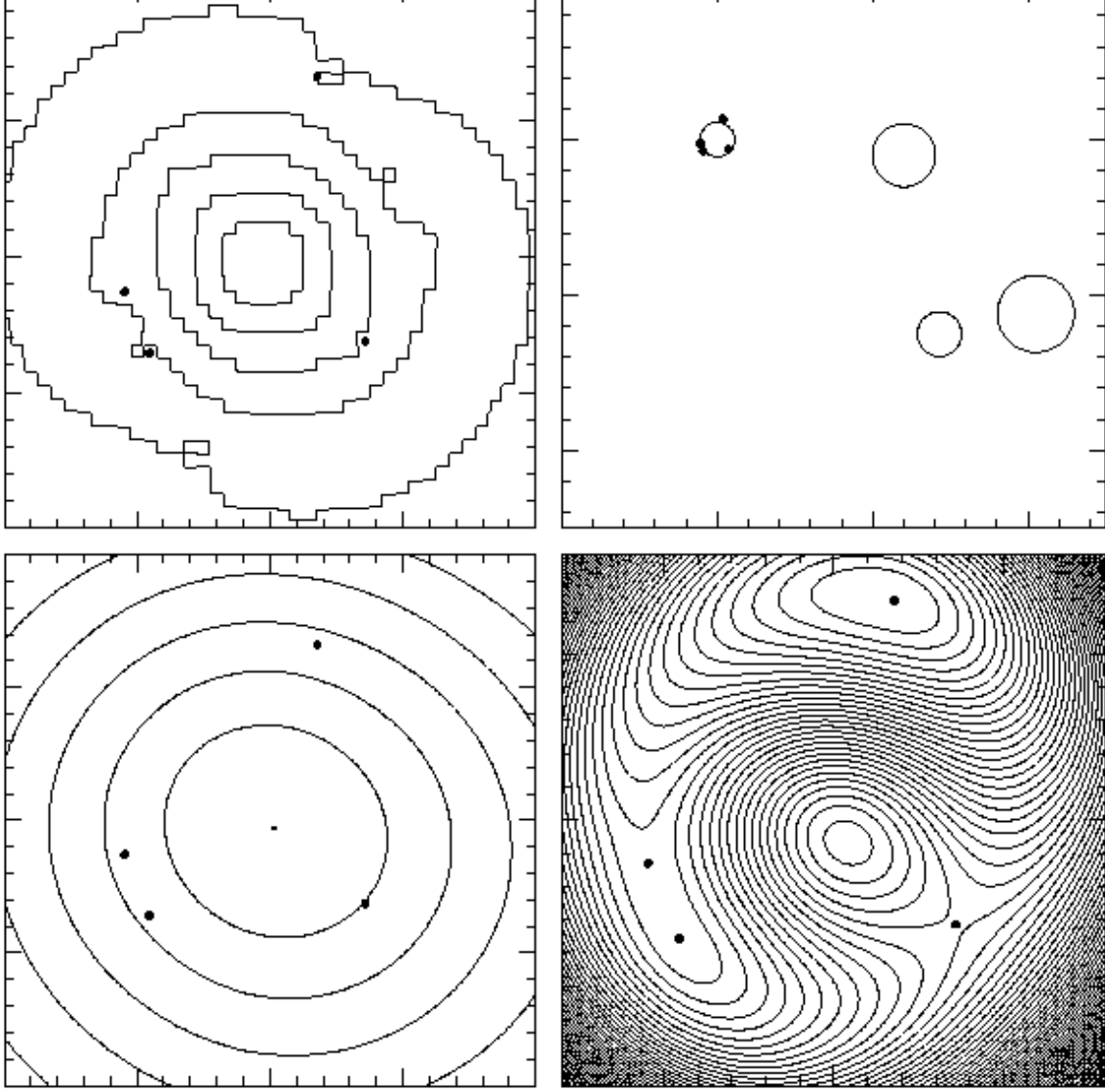
Figure 3. A reconstruction constrained by the image positions from K93 and the time delays from BK97's re-analysis of S97, and by $h = 0.42$.

The four panels follow the plan of Figure 2, except that in the upper right panel the galaxy masses are indicated by formal Einstein rings (see equation 10).

in clusters are aligned with clusters' major axis (Trevese *et al.* 1992, Fong *et al.* 1990). Similar observational evidence for poor clusters and groups is less conclusive; Mendes de Oliveira & Hickson (1994) based on a sample of ~ 100 Hickson's compact groups show that BCGs are not preferentially aligned with groups' axis. However, in our case it is the alignment of a non-BCG with the group's major axis that is of interest, and to our knowledge there is no observational data in this regard. Ciotti & Dutta (1994) performed numerical simulations to determine whether clusters' tidal field can produce alignment in elliptical galaxies located outside clusters' core. They find that an initially elliptical galaxy gets aligned with clusters' major axis due to the tidal field of a spherical cluster. However, it is still unclear if such an alignment would take place in a galaxy group. We remark that the boxy appearance of our galaxy mass maps are not entirely dissimilar from the isodensity profiles obtained by Ciotti & Dutta (see their Figures 8
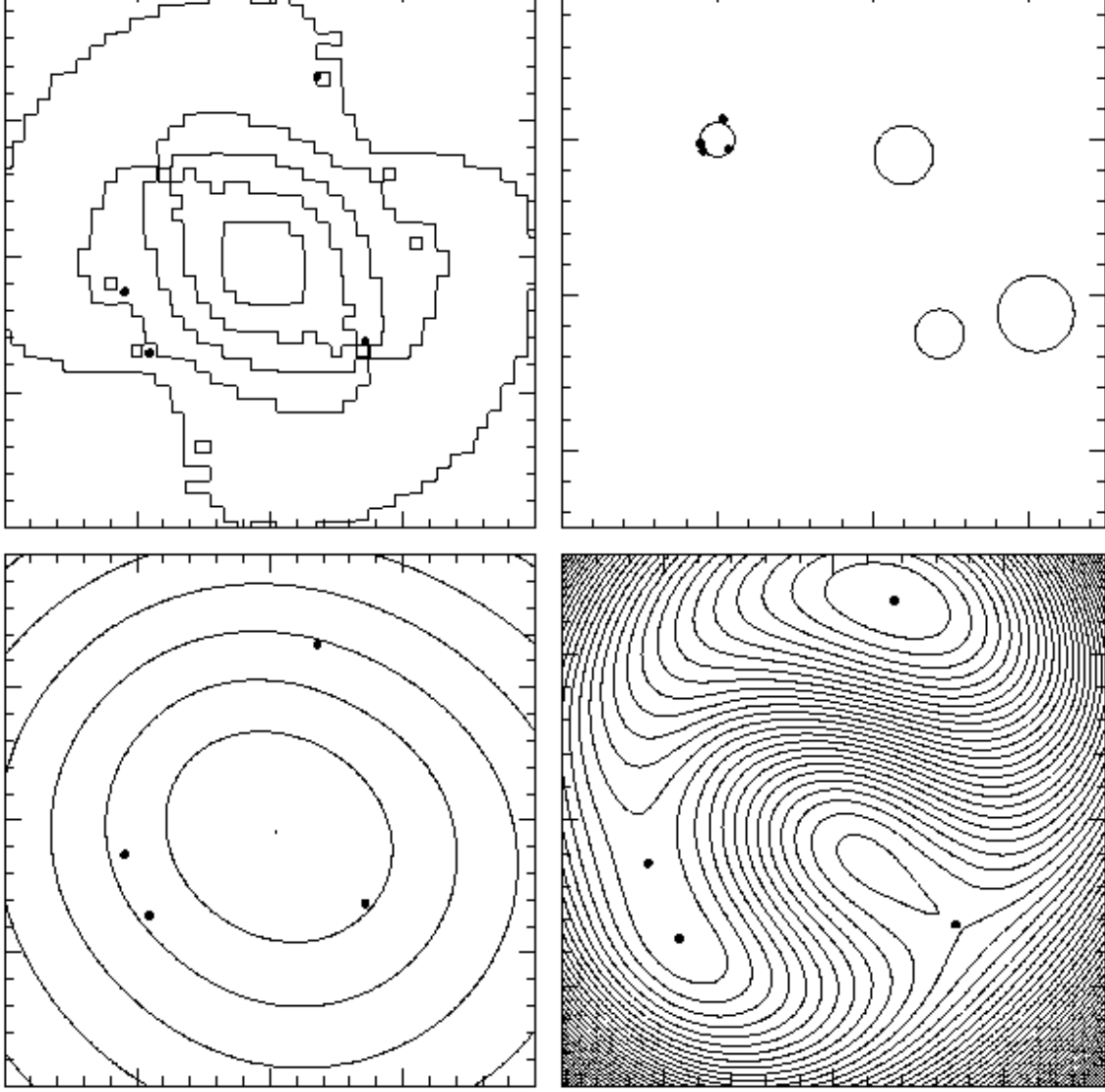
Figure 4.   Like Figure 3, except that $h = 0.63$.

and 9). Thus the alignment of the major axes of the lensing galaxy's major and its parent group are not necessarily unphysical.

Figures 3–5 indicate that higher values of h require more elliptical mass distribution in the lensing galaxy. This can be intuitively understood as follows. The time delay between any two images, $[(1+z_{\rm L})D_{\rm L}D_{\rm S}/cD_{\rm LS}] \cdot [\tau(\boldsymbol{\theta}_1) - \tau(\boldsymbol{\theta}_2)]$, where $\tau(\boldsymbol{\theta})$ is given by equation (3), is inversely proportional to h. Since time delays are fixed by observations, a higher value of h necessitates the scaled time delays, $\tau(\boldsymbol{\theta}_1) - \tau(\boldsymbol{\theta}_2)$ to be proportionately larger. The scaled time delays between roughly equally spaced (quadruple) images tend to be larger for elliptical lenses: The time delay surface consists of a geometrical and gravitational part (see equation [3]), that are added together. The images are formed at stationary points of the resulting surface, and the time delay between them is just the difference in the 'height' of the time delay surface at the image points. Then one can see that in general, when the gravitational potential of an elliptical lens is added to the geometrical part, the resulting stationary points will lie at more varied heights,
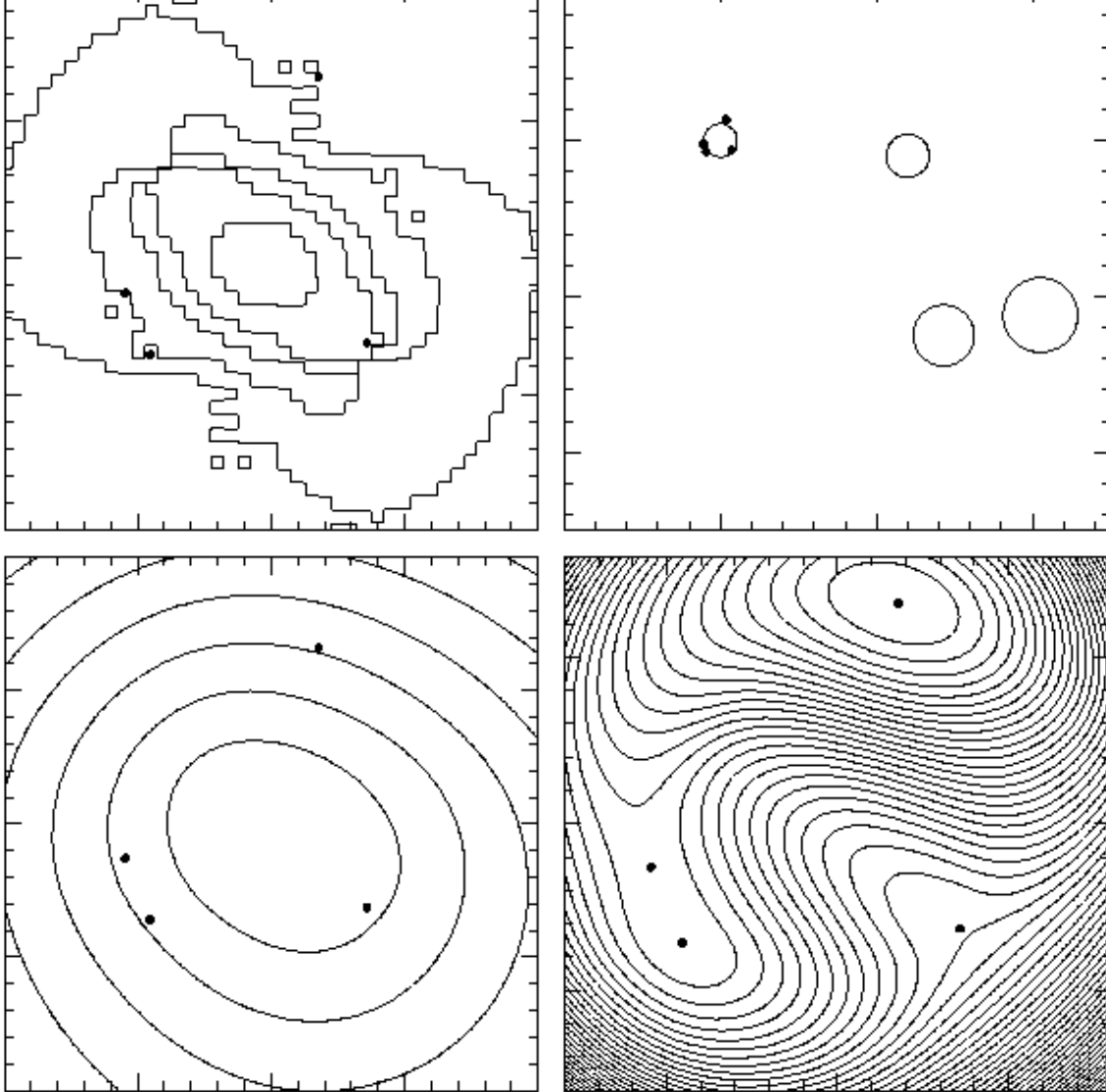
Figure 5. Like Figures 3 and 4, except now $h = 0.84$.

implying larger scaled time delays, compared to a case with a circularly symmetric lens. Therefore, more elliptical lenses require larger h, if the observed time delays are fixed.

5. CONCLUSIONS

In a multiple-image QSO, the time delay between two images can be written as

$$H_0^{-1} D(z, q_0) F_{\text{lens}}$$

where $D(z, q_0)$ is a dimensionless factor depending on the source and lens redshifts and (weakly) on q_0, and F_{lens} is of order the image separation but its exact value depends on the distribution of the lensing mass. The uncertainty in H_0 estimates from lensing comes almost entirely from the uncertainty in F_{lens}. The recent measurement by S97 of time delays in PG1115+080 are an important advance, because positions of four images, rather than two, and time delay measurements between two pairs of images, rather than one pair help constrain F_{lens} much better than in two-image systems, like Q0957+561 A&B.

Several authors have published parametric model fits to the PG1115 system; we may roughly summarize their experience as follows.

(i) A simple model suffices for a rough fit to the image positions, but to the best available astrometry one needs external shear (such as from the other group galaxies).

(ii) Fitting the time delay ratio $t_{\text{AC}}/t_{\text{BA}}$ is much more difficult; fits vary from marginally consistent to inconsistent.

(iii) Different models give very different values of H_0. In particular, the model fits in S97 give H_0 ranging from 42 to $84\,\text{km}\,\text{s}^{-1}\,\text{Mpc}^{-1}$, though the lower value is argued as more plausible.

These points prompted us to think that maybe the parametric models tried so far are only exploring a small part of 'model space', to know for sure we would have to try non-parametric models.

We have therefore developed a non-parametric or free-form lens modelling technique, which turns out to be rather simple to do. Image positions and time delay ratios constrain a pixellated mass distribution through linear equations. Assumptions like 180° rotation symmetry and density gradient always pointing inwards are also readily cast as linear constraints. Implementing all this, we find that it is almost embarrassingly easy to fit the lensing data for any plausible H_0 with plausible looking models.

We then try to pose a somewhat different question: what do different ranges of H_0 imply about the lensing galaxy that might possibly be distinguished by detailed observations of it? (At present only a centroid and a circular model for the galaxy light profile are available, from K93.) Some indications might be given by examining mass models that, while satisfying the lensing data, follow the light as closely as possible. We construct such models for $h = 0.42$, 0.63 and 0.84. The $h = 0.42$ model has a mildly elliptical mass profile with some twist in the isodensity contours. The $h = 0.63$ model has significant ellipticity inwards of the images, and the $h = 0.84$ still more. In both cases the surface density rises sharply very near image C and then flattens. Such a system could be a late elliptical, but a nearly edge-on disc would be more likely. That the $h = 0.63$ and $h = 0.84$ models have their flattening aligned with the group direction may or may not be a physical feature of some outlying members of galaxy clusters and groups. Another possibility is that the lensing galaxy is a merging system, and for $h = 0.63$ and 0.84 our density gradient condition has forced the reconstruction into an awkward shape.

In summary, the value of H_0 derived from PG1115 system and the morphology of the main lensing galaxy are degenerate. A round lensing galaxy implies low H_0, high ($> E5$) ellipticity oriented with the group direction implies high H_0.

REFERENCES

Angonin-Willaime M.-C., Hammer, F., & Rigaut, F. 1993, in *Gravitational Lenses in the Universe*, eds. J. Surdej, D. Fraipont-Caro, E. Gosset, S. Refsdal, & M. Remy (Liège: Institut d'Astrophysique), p. 85

Bar-Kana, R. 1997, Preprint, also available as astro-ph/9701068 (BK97)

Blandford, R., & Narayan, R. 1986, ApJ, 310, 568

Ciotti, L., & Dutta, S. N. 1994, MNRAS, 270, 390

Christian, C. A., Crabtree, D., & Waddel, P. 1987, ApJ, 312, 45

Courbin F., Magain, P., Keeton, C. R., Kochanek, C. S., Vanderriest, C., Jaunsen, A. O., & Hjorth, J. 1997, A&A Letters, in press, also available as astro-ph/9705093

Fong R., Stevenson P. R. F., & Shanks, T. 1990, MNRAS, 242, 146

Foy, R., Bonneau, D., & Blazit, A. 1985, A&A, 149, L13

Green, R. F., Schmidt, M., & Liebert, J. W. 1986, ApJS, 61, 305

Hege, E. K., *et al.* 1981, ApJL 248, L1

Henry, J. P., & Heasley, J. N. 1986, Nature, 321, 139

Jacoby, G. H., *et al.* 1992, PASP, 104, 599

Keeton, C. R., & Kochanek, C. S. 1997, Preprint, also available as astro-ph/9611216

Kochanek, C. S. 1991, ApJ, 373, 354

Kristian, J. *et al.* 1993, AJ, 106, 1330 (K93)

Kundić, T., Cohen, J. G., Blandford, R., D., & L. M. Lubin. 1997, Preprint, also available as astro-ph/9704109

Mendes de Oliveira, C., & Hickson, P. 1994, ApJ, 427, 684

Michalitsianos, A. G., Oliversen, R. J., & Nichols, J. (1996) ApJ, 461, 593

Narasimha, D., Subramanian, K., & Chitre, S. M. 1982, MNRAS, 200, 941

Schechter, P. L., *et al.* 1997, ApJL, 475, L85 (S97)

Shaklan, S. B., & Hege, E. K. 1986, ApJ, 303, 605

Tonry, J. L. 1997, Preprint, also available as astro-ph/9706199

Trevese D., Cirimele G., & Flin, P. 1992, AJ, 104, 935

Tripp, T. M., Green, R. F., & Bechtold, J. 1990, ApJL, 364, L29

Vanderriest, C., Vlerick, G., Lelievre, G., Schneider, J., Sol, H., Horville, D., Renard, L., & Servan, B. 1986, A&A, 158, L5

Weymann, R. J., Latham, D., Angel, J. R. P., Green, R. F., Liebert, J. W., Turnshek, D. A., Turnshek, D. E., & Tyson, J. A. 1980, Nature, 285, 641

Witt, H.-J., & Mao, S. 1997, Preprint, also available as astro-ph/9702021

Young, P., Deverill, R. S., Gunn, J. E., Westphal, J. A., & Kristian, J. 1981, ApJ, 244, 723

APPENDIX

This short appendix is about the integrals (2) over square pixels to give the contribution of one pixel to the lens potential and bending angles at arbitrary $\boldsymbol{\theta}$.

Below we will freely use cartesian or polar forms for the two dimensional angle $\boldsymbol{\theta}$.

To work out the definite integrals (2), it is convenient to first work out the indefinite integrals, which are

$$
\begin{aligned}
\widetilde{\psi} &= \frac{1}{2\pi}\Big(x^2 \arctan(y/x) + y^2 \arctan(x/y) + xy(2\ln r - 3)\Big), \\
\widetilde{\alpha}_x &= \frac{1}{\pi}\Big(x \arctan(y/x) + y \ln r\Big), \\
\widetilde{\alpha}_y &= \frac{1}{\pi}\Big(y \arctan(x/y) + x \ln r\Big).
\end{aligned}
\tag{A.1}
$$

The arctans are defined to range from $-\pi$ to π. We are free to add arbitrary functions $f(x)$ and $g(y)$ to any of the indefinite integrals (A.1). For example $2\pi\widetilde{\psi} = (x^2 - y^2)\arctan(y/x) + xy(2\ln r - 3)$ is also a legitimate indefinite integral; but it is discontinuous across the x axis, and would give wrong answers if used below in (A.2).

To get the definite integrals, we take the appropriate differences of the pixel-corner values of the indefinite integrals. Thus, if the nth pixel is centred at (x_n, y_n) we have:

$$
\begin{aligned}
\psi_n(x, y) &= \widetilde{\psi}(x_+, y_+) + \widetilde{\psi}(x_-, y_-) - \widetilde{\psi}(x_-, y_+) - \widetilde{\psi}(x_+, y_-), \\
x_\pm &= x - x_n \pm a/2, \qquad y_\pm = y - y_n \pm a/2,
\end{aligned}
\tag{A.2}
$$

and similarly for $\boldsymbol{\alpha}_n$.